Available online at www.sciencedirect.com
ScienceDirect
Bioorganic & Medicinal Chemistry 16 (2008) 4378–4389
Bioorganic & Medicinal Chemistry

Computational modeling study of functional microdomains in cannabinoid receptor type 1

Angel Gonzalez,[a,*] Leonardo Sepulveda Duran,[a,b] Raul Araya-Secchi,[a] Jose A. Garate,[a] C. David Pessoa-Mahana,[c] Carlos F. Lagos[a,c] and Tomas Perez-Acle[a,d]

[a]*Centre for Bioinformatics CBUC, Faculty of Biological Sciences, Pontificia Universidad Católica de Chile, Portugal 49-6513492, Santiago, Chile*
[b]*Center for Biophysics and Computational Biology, University of Illinois at Urbana-Champaign, Urbana, IL 61801, USA*
[c]*Medicinal Chemistry Laboratory, Department of Pharmacy, Faculty of Chemistry, Pontificia Universidad Católica de Chile, Av. Vicuña Mackenna 4860-7820436, Macul, Santiago, Chile*
[d]*Fundación Ciencia para la Vida, Santiago, Chile*

Received 21 November 2007; revised 18 February 2008; accepted 21 February 2008
Available online 26 February 2008

Abstract—The seven transmembrane helices (TMH) G-protein-coupled receptors (GPCRs) constitute one of the largest superfamily of signaling proteins found in mammals. Some of its members, in which the cannabinoid (CB) receptors are included, stand out because their functional states can be modulated by a broad spectrum of effector molecules. The relative ligand promiscuity exhibited by these receptors could be related with particular attributes conferred by their molecular architecture and represents a motivating issue to be explored. In this regard, this study represents an effort to investigate the cannabinoid receptor type 1 (CB1) ligand recognition plasticity, using comparative modeling, molecular dynamics (MD) simulations and docking. Our results suggest that a cooperative set of subtle structural rearrangements within the TMHs provide to the CB1 protein the plasticity to reach alternate configurations. These changes include the relaxation of intramolecular constraints, the rotations, translations and kinks of the majority of TMHs and the reorganization of the ligand binding cavities.

1. Introduction

The so-called marijuana, *Cannabis sativa*, or hemp is one of the oldest psychoactive plants known by humanity. It has been used for delight and medical purposes, with early records of therapeutic applications in oriental cultures since ~3000 BC. Its physiological effects are mediated by the interaction of structurally diverse cannabinergic compounds[1] (see Fig. 1) with the CB1 and CB2 cannabinoid receptors.[2] Both proteins belong to the G-protein-coupled receptors (GPCRs), one of the largest and more studied superfamily of transmembrane proteins.[3] Due to their wide distribution among different body tissues, their involvement in several metabolic pathways, together with their exposition to the extracellular environment, GPCRs represent the most important target class of proteins for drug discovery.[4]

Available evidence supports the notion that all GPCRs share a common fold. Their general architecture is defined as a counterclockwise arrangement of seven transmembrane alpha-helices (TMHs) of ~25 to 35 residues long (TMHs 1 to 7), which span the cellular membrane connected by three extracellular (EC 1 to 3) and three cytoplasmatic loops (IC 1 to 3).[5–7] The N-ter-

Abbreviations: CB, cannabinoid receptor; GPCR, G-protein-coupled receptors; TMH, transmembrane helices; EC, extracellular loop; IC, cytoplasmatic loop; R, CB1 model derived from rhodopsin; R*, CB1 model obtained from R; MD, molecular dynamics; SA, simulated annealing; CG, conjugate gradient; RC, rotating constraint; POPC, 1-palmitoyl-2-oleoyl-*sn*-glycerol-3-phosphatidylcholine; PME, particle mesh Ewald; RMSD, root mean square deviation; RMSF, root mean square fluctuation; LGA, Lamarckian genetic algorithm; $\chi 1$, $\chi 1$ dihedral angle; $g\pm$, gauche ± conformation; AAI, aminoalkylindole; Nap, naphtyl group; Ind, indole; Morph, morpholinyl; Pyr, pyrazole; Carbx, carboxamide; MC, 4-chlorophenyl; DC, 2-4-dichlorophenyl; Pip, piperidine; SAH, southern aliphatic hydroxyl; SAC, southern aliphatic chain.

Keywords: Cannabinoid receptor; CB1; GPCR; Activation mechanism; TMH; Ligand binding; Docking; Conformational changes; Comparative modeling; Molecular dynamics.

* Corresponding author. Tel.: +56 2 686 2269/686 2268; fax: +56 2 686 2900; e-mail addresses: angel@cbuc.cl; angellox@gmail.com

0968-0896/$ - see front matter © 2008 Elsevier Ltd. All rights reserved.
doi:10.1016/j.bmc.2008.02.070

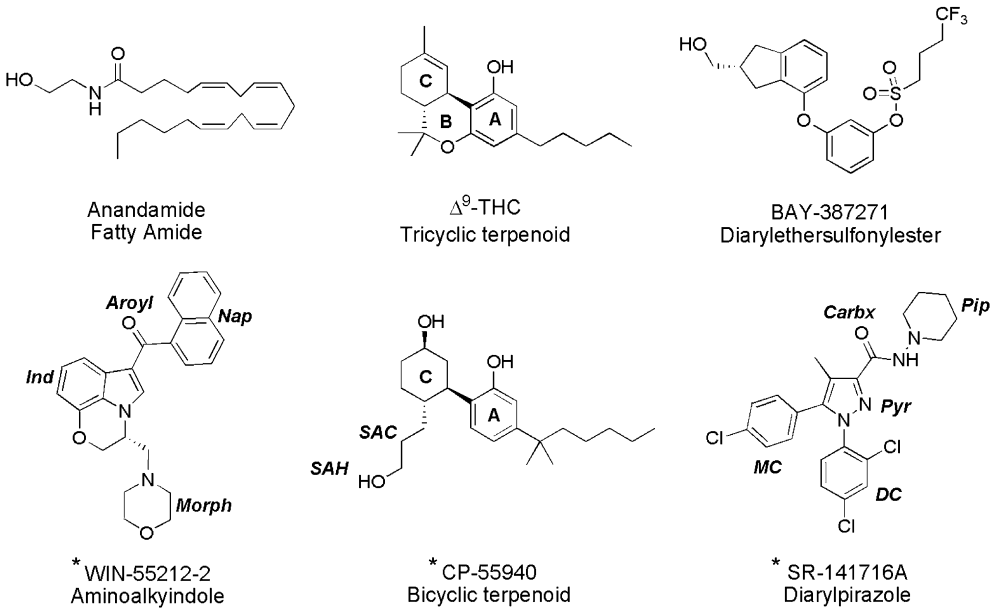

Figure 1. Structural diversity of some cannabinergic compounds. Representative ligands used in dockings experiments appear marked with an asterisk (*). Abbreviations for ligands functional groups are shown in italics.

minal region, which varies in length and function, is located on the extracellular side of the membrane, while the C-terminal region is on the intracellular side. In addition to the characteristic 7 TMHs, some GPCR class A family members like rhodopsin, $\beta_{1/2}$-adrenergic and CB receptors have a short C-terminal helix (helix 8) that lays on the cytoplasmatic side of the lipid bilayer.[8–11]

At present time, the existence of crystallographic X-ray data of the bovine rhodopsin has allowed the development of a broad spectrum of comparative models for other GPCR family members.[12,13] This approximation has been successfully used to identify functional or structural characteristics of other GPCRs, and in some cases has contributed in the understanding of their activation mechanism.[12,14] In this regard, most accepted hypotheses support the notion that most GPCRs exist as a collection of states in the conformational space described by several multi-state ensembles.[15,16] The conformational plasticity exhibited by these receptors permits their interaction with an extraordinary diversity of ligands in the extracellular regions, whereas conformational rearrangements take place in the cytoplasmatic regions near the G-protein binding domain during the activation process.[17]

In this study our primary motivation is to expand the current knowledge regarding CB1 ligand recognition plasticity, through the use of biophysical computational tools. In accordance with our results, it is possible to produce alternative conformations of a CB1 molecular model derived from the inactive rhodopsin that conserve the affinity for ligands in docking experiments. Differences between these conformations reveal a reorganization of ligand binding sites that could be used to define separate functional modules within this protein; the cytoplasmatic and extracellular subdomains, and the aromatic and polar microdomains.

2. Methods

2.1. Development of a CB1 molecular model (R)

In order to produce a CB1 inactive molecular model (R), the 2.8 Å crystal structure of bovine rhodopsin was used as template for comparative modeling.[8] CB1 and rhodopsin sequences were aligned using the available information of highly conserved residues shared within the GPCRs.[18] The N-(amino acids 1–105) and C-terminus (amino acids 415–472) residues of CB1 sequence were the only omitted regions (see Discussion). The produced alignment was similar to the one reported by Salo et al.[19] This alignment was used as input to MODELLER v8 [20] to develop a total of 100 comparative models that were evaluated using PROSA II[21] and Verify 3D.[22] The best evaluated structure was selected for further refinement. Loops regions were optimized through a MD Simulated Annealing (SA) protocol. For this purpose, backbone residues of TMHs and helix 8 were constrained and loops conformation were optimized in 3 (SA) cycles of heating up to 700 K and slowly cooling down to 300 K in successive 10 K, 20 ps steps followed by a conjugate gradient (CG) energy minimization using CHARMM22 forcefield.[23]

2.2. The CB1 (R*) model

To generate a second conformation (R*), which could be associated to a putative active state of CB1, the TMH3 and 6 of the R model were perturbed using the rotating constraint (RC) module implemented in NAMD v2.5.[24] The procedure was conducted by the harmonic constraint of TMHs 3 and 6 Cα atoms to reference axes that were rotated with a constant angular velocity (Ω) of 0.001 degrees/timestep. The rotation axis for TMH3 was defined as a tilted vector in the *z*-axis passing through the helix center of mass. For

TMH6, we used a vector sum between the two helix axes defined by the $CWGP_{6.50}$ kink region. To achieve a uniform rotation and to avoid alpha helical distortions, the procedure was repeated adjusting the magnitude of the constraint forces applied in a range of 0.2 to 1 kcal mol^{-1} $Å^{-2}$ relative to each atom distance from the rotation axes until a regular rotation was achieved.[25] During the simulation, backbone atoms of the remaining helices were held fixed and loops were free to move. The simulation was carried out using the CHARMM22 forcefield during 1 ns in vacuum with a dielectric constant value of 2, followed by a CG energy minimization until convergence.

2.3. Membrane simulations

The R and R^* models were independently embedded in a pre-equilibrated lipid bilayer consisting of 128 molecules of 1-palmitoyl-2-oleoyl-*sn*-glycerol-3-phosphatidylcholine (POPC).[26,27] Insertion of the alpha helical bundle into the lipid core was adjusted to obtain both the TMH4 and the cytosolic half of TMH6 perpendicular to the membrane plane[8,28] and protein-overlapping lipids were removed. Final POPC-R (see Fig. 2) and POPC-R^* systems dimension resulted in a box of $62 \times 62 \times 97$ (Å) with a total of 26,272 atoms. Simulations were carried out using GROMACS v3.0 MD package.[29] Lipid parameters were taken from Berger et al.[26] combined with the SPC water model. Long-range electrostatic interactions were calculated using the particle mesh Ewald method (PME) to get a uniform density average area per lipid during simulation.[30] Lennard-Jones and short-range neighbor list for Coulombic interactions were set at 1 nm. Simulations were performed applying a constant pressure in all directions of 1 bar with a coupling constant of $p = 0.5$ ps and a compressibility of 4.5×10^{-5} bar^{-1}. To compensate for net charge of the systems, 15 Cl^- ions were added. Temperature was controlled by independently coupling the protein, lipids, solvent and counter-ions to a 310 K temperature bath using Berendsen algorithm with a coupling constant of 0.1 ps.[31] Energy minimization to reduce close contacts was achieved through the steepest-descent algorithm, until the maximum force decayed to 100 [kJ mol^{-1} nm^{-1}]. Final energy minimized systems were then pre-equilibrated as shown in Table 1. Later, the three resulting systems were subjected to a 10 ns MD simulation run at 310 K with 1 fs timestep.

2.4. Conformational changes analysis

The minimized, post-MD R and R^* structures were used to carry out structural comparisons. Helix boundaries were defined according to DSSP program[32] using as reference the initial R model. The root mean square deviation (RMSD) between R and R^* was calculated both globally, using an all-residue C_α RMSD fit, and locally, by fitting secondary structure elements separately, as shown in Table 2. A displacement profile ($C\alpha^{R*}$-$C\alpha^{R}$) was also computed for the global and local RMSD superimpositions. Global Cα displacement profile was used to measure the overall differences within the models, while the local displacement profile was used to discriminate between rigid-body movements or TMHs disruption. TMHs displacement angles were calculated as the angle difference between the least square fit vectors passing through the helix Cα atoms in each conformation. TMHs movements in *z*-axis were calculated as the average *z*-axis displacement of its constituents Cα atoms. RMSDs, Cα displacements, vector definitions, changes on helices orientation, and *z*-axis displacements were calculated using the Tcl scripting capabilities implemented on VMD.[33]

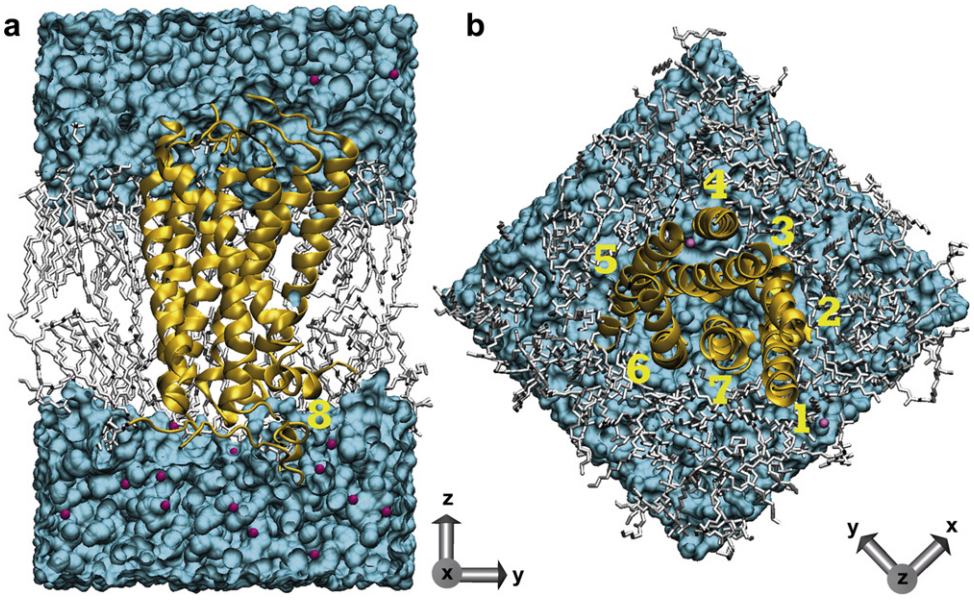

Figure 2. POPC-CB1 molecular system. Lateral (a) and extracellular (b) views of the POPC-R system after 10 ns MD simulation. CB1 receptor appears in golden ribbons and lipids in gray licorice. A solid blue surface represents water molecules and ions are represented in magenta. Axes appear in the lower right corner.

Table 1. Pre-relaxations schemes applied to the membrane-protein systems prior to the 10 ns collection phase of MD runs. POPC-R, system composed by 96 1-palmitoyl-2-oleoyl-*sn*-glycerol-3-phosphatidylcholine molecules, 15 chloride ions, and the CB1 starting model (R) (see Figure 2)

Systems	Time (ps)	Isotropic force constants (kJ mol^{-1} nm^{-2})	Constraint forces applied to TMHs
POPC-R (a)	500	1000	Heavy atoms
	350	—	—
POPC-R** (b)	500	1000	Heavy atoms
	350	—	—
POPC-R* (c)	500	1000	Heavy atoms
	300	1000	Backbone atoms
	300	1000	TMHs 3 and 6 backbone atoms
		500	TMHs 1, 2, 4, 5, 7 backbone atoms
	300	1000	TMHs 3 and 6 backbone atoms
		250	TMHs 1, 2, 4, 5, 7 backbone atoms
	300	1000	TMHs 3 and 6 backbone atoms
		50	TMHs 1, 2, 4, 5, 7 backbone atoms
	350	—	—

The POPC-R* and POPC-R** systems differ in the releasing of constraints applied to the CB1 model (R*).

Table 2. Structural comparisons between the CB1 R and R* minimized structures after the 10 ns MD run

Structure	Residues			RMSD (Å)		Angle[c] (degrees)	Δ*z*-axis[d] (Å)	SASA[e] (Å^2)		
	Start	End	Total	Global[a]	Local[b]			R	R*	ΔSASA
TMH1	113	142	30	2.3	1.3	3.2	−0.8	1547.0	1631.9	84.8
TMH2	151	179	29	2.6	2.0	4.5	−0.1	721.2	741.1	19.8
TMH3	187	217	31	3.1	2.5	4.0	−0.7	557.0	702.2	145.2
TMH4	229	250	22	1.6	0.5	5.9	−1.0	1414.7	1411.8	−2.9
TMH5	274	297	24	3.3	0.9	5.6	2.4	1285.9	1311.5	25.6
TMH6	338	367	30	3.3	1.3	7.4	2.0	1248.9	1522.1	273.2
TMH7	377	400	24	3.2	2.2	8.2	0.9	782.5	674.8	−107.7
H8	402	411	10	3.4	0.4	29.5	−3.6	464.4	525.6	61.1

[a] RMSD values after an all-atom RMSD fit.
[b] RMSD after singly fit each secondary structural region.
[c] Relative TMHs angles displacement after an all-atom RMSD fit.
[d] TMHs *z*-axis displacement after an all-atom RMSD fit.
[e] Solvent accessible surface areas.

The change in secondary structure of residue *i* was calculated according to the following equation:

$$\Delta\text{Angle}_i = \left| \frac{(\phi_i^{R^*} - \phi_i^{R}) + (\psi_i^{R^*} - \psi_i^{R})}{2} \right|$$

where $\phi_i^{R^*}$ and $\psi_i^{R^*}$ are the phi and psi angles of residue *i* in the R* model. The change in the number of contacts made by residue *i* was computed using the following equation:

$$\Delta\text{contacts}_i = \sum_{\substack{i=1 \\ i-1>j>i+1}}^{308} c_{ij}^{R^*} - c_{ij}^{R}$$

where $c_{ij}^{R^*}$ and c_{ij}^{R} are the number of contacts between residues *i* and *j* in R* and R, respectively. Two atoms were considered in contact if they were at most 6 Å apart.

2.5. Conservation index calculation

A multiple sequence alignment of GPCR rhodopsin-like superfamily (1883 sequences)[18] was used to correlate sequence conservation with conformational changes in CB1 receptor. We calculated a conservation index (C_i), based on the well-known Shannon's Entropy[34,35] equation as follows:

$$C_i = 100 \times \left(1 + \frac{1}{\log(20)} \sum_{k=1}^{20} p_{ik} \log(p_{ik})\right)$$

where, p_{ik} denote the relative frequency of the residue *k* in the alignment position *i*. For conserved positions ($p_{ik} \sim 1$) the conservation index is maximum ($C_i \sim 100$). On the contrary, for non-informative columns where all residues are uniformly distributed ($p_{ik} \sim 1/k$), C_i reaches a minimum conservation value ($C_i \sim 0$). Backbone angles, contacts, and conservation calculations were made through Perl Scripts.

2.6. Docking studies

Docking studies were carried out using AUTODOCK 3.0.5[36] and AutoDockTools using as receptors the R and R* post-MD models. Ligand molecules were constructed using standard bond lengths and angles from InsightII/Builder module[37] and then optimized at HF/6-31g* quantum mechanical theory level using Gaussian03 program.[38] AutoDockTools were used to identify ligand's aromatic carbons, to assign the rigid root, ac-

tive torsions, and to merge non-polar hydrogens to their parent atoms. For each receptor model, docking grids comprised the entire extracellular half section of the TMHs bundle. The Lamarckian genetic algorithm (LGA) available in Autodock was used to explore the conformational space accessible to ligands. For each ligand, docking simulation was composed of 100 independent runs, starting each one from a random conformation. Ligand–receptor complexes were energy minimized and evaluated using the empirical scoring functions available from the Ludi algorithm.[39,40] In order to describe ligand binding interactions, the lowest energy representatives of the different binding modes were selected for further analysis.

3. Results and discussion

3.1. The CB1 R model

The CB1 extracellular N-terminal domain is uncommonly long among the various members of class A GPCRs and seems to play no role in ligand binding or receptor activation.[41] This region together with the intracellular C-terminal domain constitutes the least conserved regions of the receptor when compared to the rhodopsin template and were omitted in the modeling protocol. The rest of the sequence, including loops, were modeled and further optimized as described in methods. Most of the class A GPCRs family members (>90%) have a disulfide bridge between the TMH3 and the extracellular loop 2 (EC2), the CB receptor subfamily being an exception. However, there are evidences of a disulfide bridge between C_{257} and C_{264} residues in CB receptors[42,43] and was included in our modeling protocol.[44] As a result of imposing this restraint, the EC2 loop bends over the receptor core in a similar way as is found in rhodopsin.

At the cytoplasmatic region, the amphiphatic helix 8 (also called fourth cytoplasmatic loop, residues 402 to 411) lay perpendicular to the TMHs, with polar residues K_{402}, D_{403}, H_{406} and S_{410} facing the solvent and hydrophobic residues in close contacts with the lipid phase.[10] Later, as a consequence of the SA loop refinement step, the solvent accessible residues located in helix 8 established contacts with R_{336}, D_{324}, E_{323} and S_{322} IC3 loop residues. These interactions were kept throughout the 10 ns MD simulations, leading to the arrangement of the IC3 C-terminal region (residues 315 to 337) and the helix 8 in a double-bow structure in which all residues reported to be involved in G protein sequestration resulted in close proximity[45] (see Fig. 8). Verify-3D results and PROSA energy evaluation of developed models were equivalent to those of rhodopsin (see Supplementary Material), supporting the idea (albeit differences) that this template structure is a useful starting point to conduct a structural characterization of the CB1 receptor.[13]

3.2. The CB1 R* model

Empirical evidence supports the notion that TMH 3 and 6 have an important role in the activation of various class A GPCRs.[46–49] Indications derived from diverse experiments suggest that activation could include the breaking of a salt bridge at the intracellular ends of TMHs 3 and 6,[50] the counterclockwise rotations of these two helices,[51] and the straightening of the proline kink in TMH6.[52] This knowledge has been used to produce active conformations of CB1 molecular models.[13,53–55] Thus, an alternative CB1 model (R*) was built from the initial R model coordinates to reproduce the conformational changes suggested to occur during receptor activation.[13] In order to reproduce these changes, TMH3 and 6 in the R model were rotated (~20 degrees) using the RC tool implemented in NAMD. This technique has the benefit to consider the effect of the surrounding helices during the rotation process and the option to modify the rotating constraints force in order to avoid dihedral angles distortions or secondary structure loss.[25] As a result, heavy atoms RMSD (including loops) was less than 3 Å between the initial (R) and the final (R*) structures. It is important to mention that according to the GPCR multi-ensemble theory,[15] the selection of a single structure as a representative of the

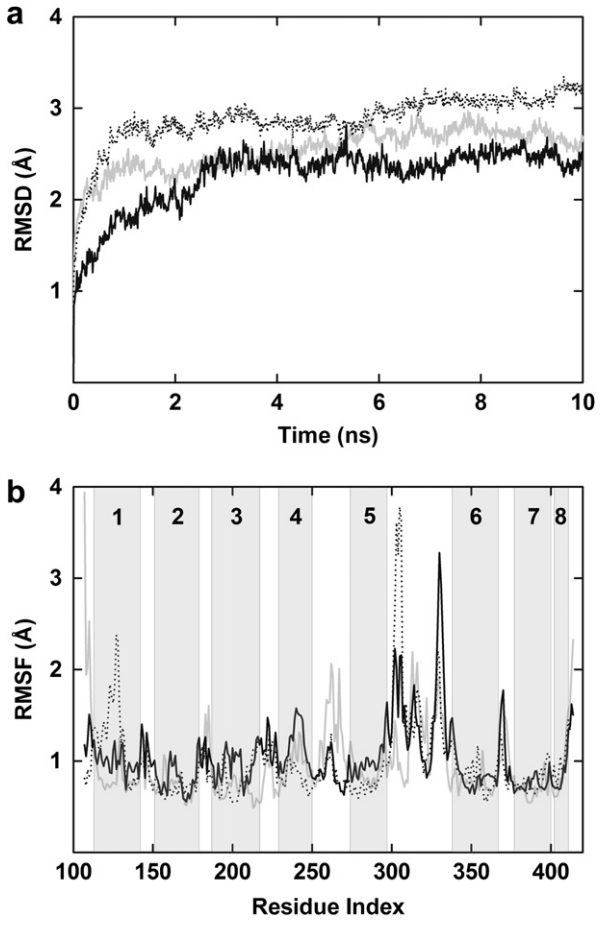

Figure 3. Molecular coordinates displacements for the R (gray line), R* (black continuous line), and R** (black doted line) during the POPC MD simulations. (a) The root mean square deviation (RMSD) of backbone protein atoms during the 10 ns of simulation. (b) The root mean square fluctuation (RMSF) values for every residue Cα atoms. The secondary structure alpha helical topology elements are denoted by gray bars with numerals.

activated form constitutes a simplification. However, for the scope of this work, the comparison between two states provides a valuable framework to analyze the most responsive structural regions to conformational changes that could occur within the CB receptor as well as in the ligand binding pockets (see below).

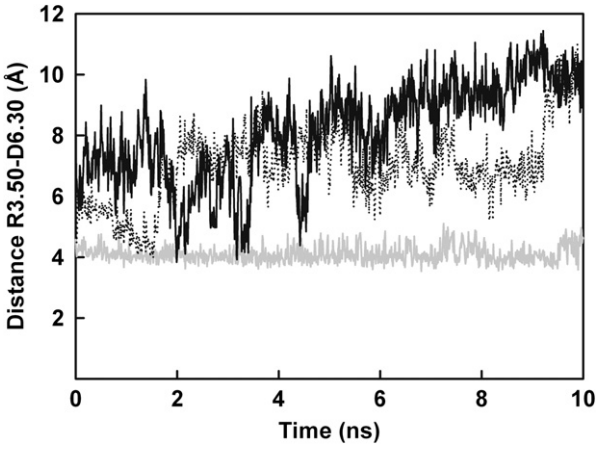

Figure 4. The 'ionic lock' residues. Distances between the $R_{3.50}$ guanidinium group and the $D_{6.30}$ carboxylic group during the 10 ns POPC MD simulations. R (gray line), R^* (black continuous line), and R^{**} (black doted line).

3.3. MD simulations in explicit membrane

MD simulations for both R and R^* models were conducted in an explicit lipid bilayer environment to reproduce a more biologically realistic condition. Tieleman's POPC pre-equilibrated membrane patch was selected on the basis of its good performance in a previous 45 ns simulation on rhodopsin dimer.[56] Pre-relaxation in the membrane environment was carried out as shown in Table 1. The sequential relaxation scheme applied to the POPC-R^* system (see Table 1c) was designed in order to offset the restriction imposed to the TMHs 1-2-4-5-7 during the rotation of TMH3 and 6. Thus, helices constraints were diminished in successive steps to avoid undesirable structural drifts during production. In addition, for comparison purposes, an extra simulation was conducted to the POPC-R^* system (named POPC-R^{**} as shown in Table 1b) using the simplified pre-equilibration protocol employed on the POPC-R system (Table 1a). Final relaxation for the three systems was reached close to the 2 ns simulation (see Fig. 3a).

The POPC-R, POPC-R^*, and POPC-R^{**} membrane-protein systems remained stable after relaxation as no drift in energy, temperature, or lipids density was observed during the collection stage (data not shown). The Cα RMSD values below 3 Å during the simulation time also suggest the overall structural stability of all models (see Fig. 3a), being the largest RMSF located

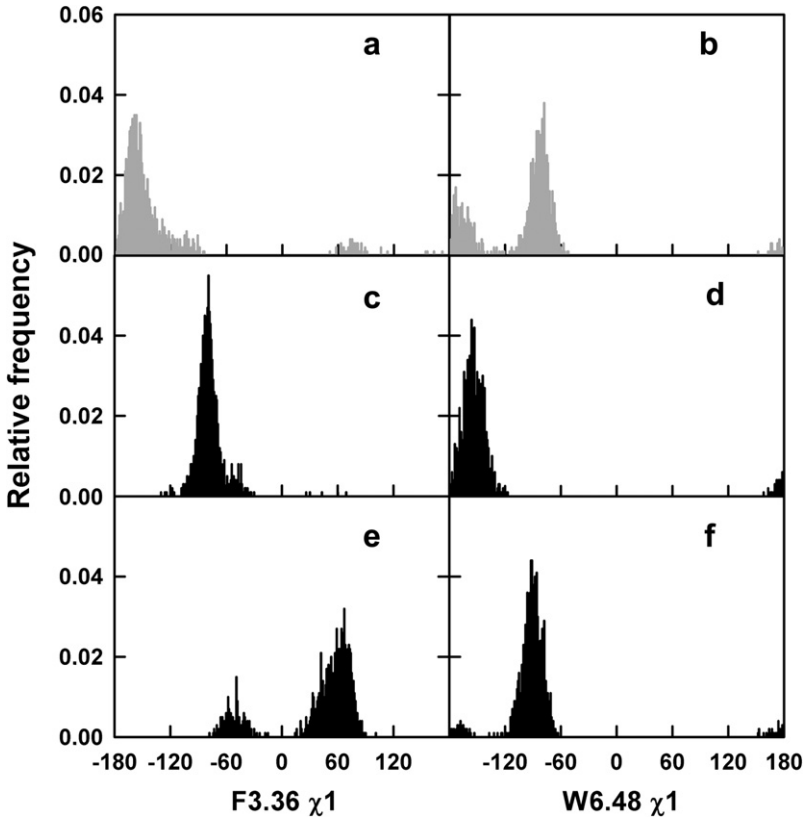

Figure 5. The 'toggle switch' residues. Cumulative frequency of $F_{3.36}$ and $W_{6.48}$ Chi ($\chi 1$) angle distributions during the collection phase of POPC MD simulations for R (a and b), R^{**} (c and d), and R^* (e and f). The torsion space is defined by the rotamer angles $g-$ ($\chi 1 = 60 \pm 60$), $g+$ ($\chi 1 = -60 \pm 60$) and *trans* ($\chi 1 = 180 \pm 60$).

in the loops (Fig. 3b). However, when comparing the RMSF plots of the R* and R** models, some important differences can be outlined. R** is the model with the largest fluctuations showing changes outside the loops that include a significant distortion in TMH1 (see Fig. 3b). In contrast, RMSD and RMSF values of R* did not show any strong distortion along its structure. This result suggests that the smooth MD relaxation applied on R* (see Table 1c) was better to circumvent helix disruptions.

3.4. Analysis of intramolecular constraints

Preliminary evidence suggests that GPCRs activation involves disruption of an ionic interaction between the cytoplasmatic ends of TMHs 3 and 6.[57] These helices are thought to be constrained by a $D/E_{3.49}$–$R_{3.50}$–$E_{6.30}$ salt bridge that limits their mobility in the inactive state. This interaction operates as an 'ionic lock' that needs to be broken to reach the active conformation.[50] Figure 4 shows the distances between $D_{6.30}$ carboxylic group and $R_{3.50}$ guanidine group during the 10 ns MD simulations in our CB1 models. In R, the distance between these residues is maintained around 4 Å, consistent with a salt bridge. On the other hand, this interaction is far beyond 6 Å in the R* and R** models. This salt bridge is not mandatory to keep CB1 in an inactive conformation and it is suggested that a more complex set of intramolecular interactions is required.[58] In this regard it has been proposed that the CB1 activation could be related to the rotameric states of the chi 1 (χ1) torsion angles of the aromatic residues $W_{6.48}$ and $F_{3.36}$ located within TMH3 and TMH6 helices.[59,60] This concomitant $W_{6.48}$ ($\chi 1 g+ \rightarrow trans$)/$F_{3.36}$ ($\chi 1 trans \rightarrow g+$) shifting was denoted the 'rotamer toggle switch' and was also tested in our models by computation of the average distribution of the $F_{3.36}$ and $W_{6.48}\chi$1 angles during the MD experiments (see Fig. 5). As can be noted, the R and R** models satisfy this hypothesis.

Additional regions within the 7 TMHs bundle have also been described as significant to the GPCRs functionality. These include the TMH1, TMH2, and TMH7, where the conserved polar residues $N_{1.50}$, $D_{2.50}$, and $N_{7.49}$ are highly relevant.[61–65] Inter-atomic distances among these residues during the MD experiments reveal them as structural constraints in our CB1 modeled structures (see Fig. 6a and b). In the CB1 R model, $D_{2.50}$ resulted close to $N_{1.50}$ as computed in Figure 6a, whereas in R* the interaction reorders to bring $N_{7.49}$ close to $D_{2.50}$ (see Fig. 6b). Therefore, a dual control of intermolecular interactions is observed throughout the structure.[66]

3.5. Conformational changes analysis

As a following step, a selection between the R* and R** models was carried out in order to simplify the comparative analysis with the primary R model derived from the inactive rhodopsin coordinates. In accordance to Figure 5, the R** model satisfied better than R* the toggle switch hypothesis. On the other hand, during the MD collection phase, R** resulted the most unstable

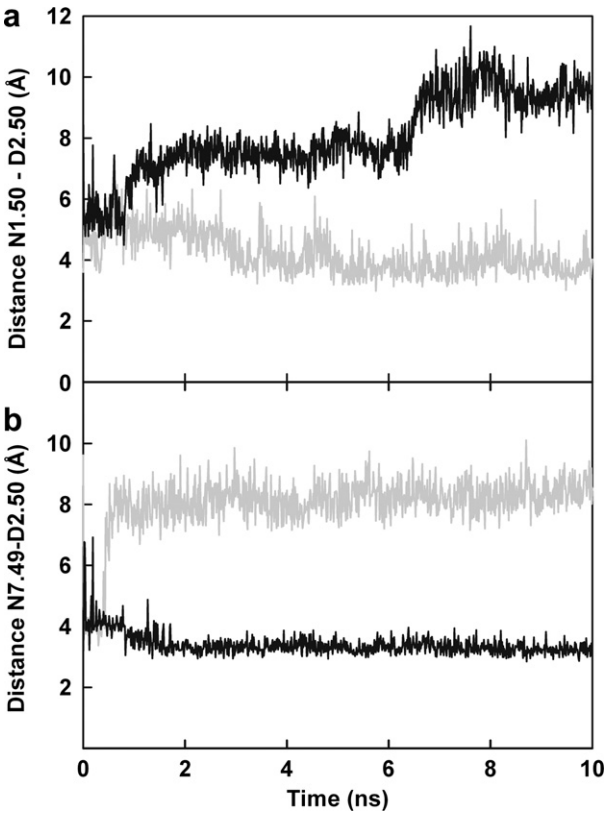

Figure 6. The 'polar pocket' residues. Distances between the $D_{2.50}$ carboxylic and the $N_{1.50}/N_{7.49}$ carboxiamide groups in the R model (gray line) and the selected model R* (black line) during the 10 ns POPC MD run.

model with some helical regions, especially TMH1, exhibiting large fluctuations (see Fig. 3a and b). Consequently, the more stable R* model was selected in further comparisons.

Global and local descriptors were calculated in order to describe the structural differences between R and R* post-MD models. Cα atom fit between R and R* gave a RMSD of 3.4 Å. Most noticeable differences in the TMHs comprise the counterclockwise/upward displacement of TMHs 5 and 6 together with the clockwise/downward displacement of TMHs 1 and 2 (see Table 2 and Fig. 7f–h). Global displacement profile values for TMHs 1, 2, and 4 were smaller than the remaining TMHs, suggesting that the latter relocate to a higher extent (see Table 2 and Fig. 7a black profile). Only TMHs 1, 4 and 5 showed a uniform local displacement profile, indicative of rigid-body movements (TMH1 and 5 lack helix-kinking proline residues). TMH2 maintains its overall conformation, but in the R* model, LA-$VAD_{2.50}$LLG residues change their backbone dihedral angles producing a bulge in the middle of the helix (see Fig. 7b and e). This change seems correlated to the $D_{2.50}$–$N_{7.49}$ polar interaction, since the TMH2 LA-$VAD_{2.50}$L motif is facing the $NP_{7.50}$IIY conserved motif in TMH7 that also changes during the simulation (see Fig. 7b and e and Fig. 8). In TMH3 two kinks were produced toward the extracellular region in R* (residues NVFLFKLGGVTAS), just before the $F_{3.36}$ toggle

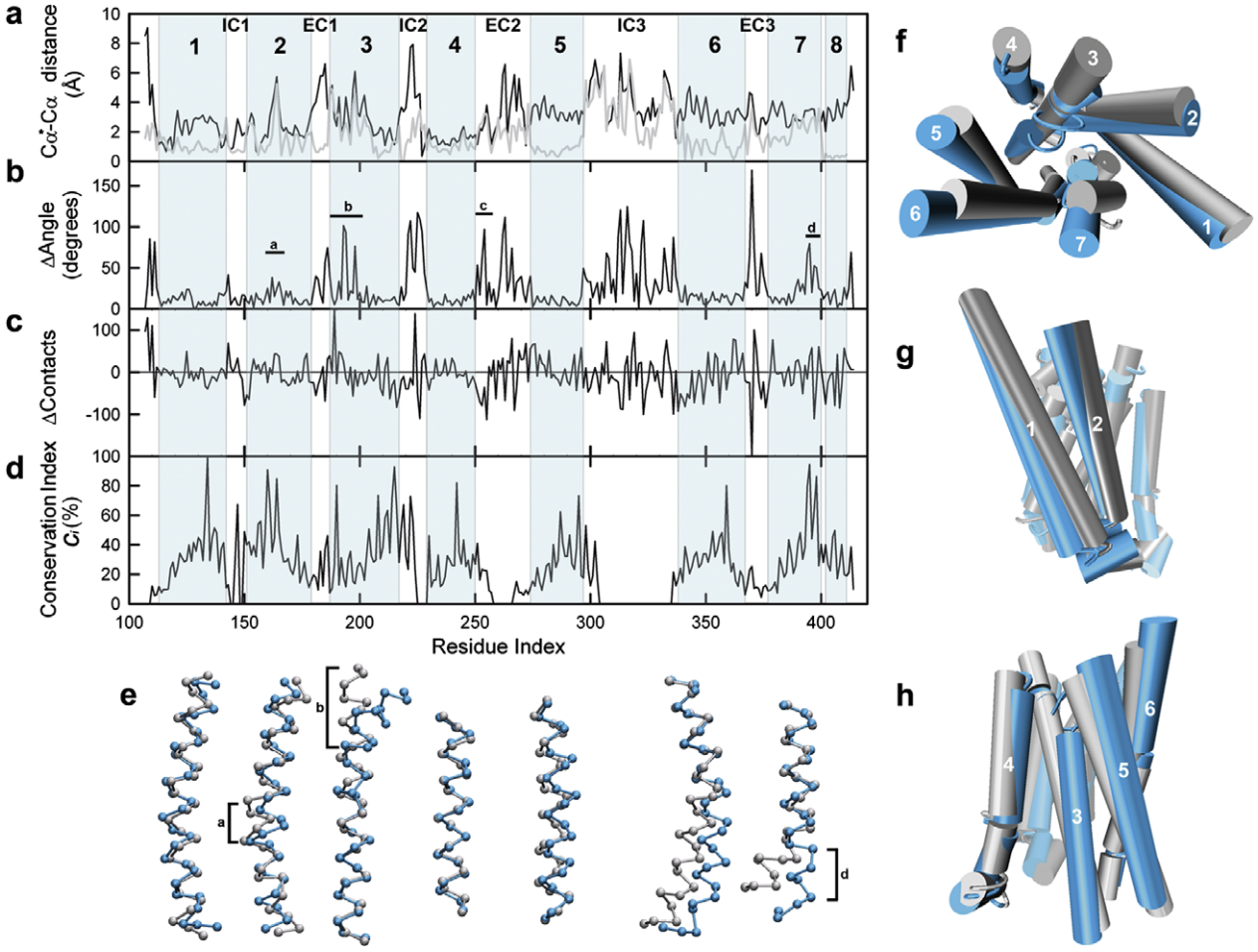

Figure 7. Structural comparisons between the final R (gray) and R* (cyan) models after 10 ns MD simulation and energy minimization. (a–d) Residue-based descriptors. (a) Distances between Cα atoms after an all-residue RMSD fit (global profile, black line) and after a secondary structure RMSD fit (local profile, gray line). (b) Changes in backbone dihedral angles when comparing R* versus R models. Horizontal bars denote (a) the TMH2 LAVAD$_{2.50}$LLG motif, (b) the TMH3 extracellular residues NVFLFKLGGVTAS, (c) the TMH4 extracellular residues PLLGWN, and (d) the P$_{7.50}$IIYA motif in TMH7. (c) Changes in the number of protein–protein atomic contacts when comparing R* versus R. (d) Conservation index obtained from a 1883 sequence alignment of the GPCRs class A rhodopsin family members. (e) Structural superposition of TMHs between R* and R models. Vertical bars correspond to the sequences depicted in the graph insets of b. (f–h) Different views of the R* and R superimposed structures. Loops are omitted for clarity. Figures were created using VMD v1.8.5.

switch component, while the conformation of cytoplasmatic residues was maintained (see Fig. 7b and e). A possible explanation to this result could be attributed to the absence in the CB1 receptor of the TMH3–EC2 disulfide bridge, and by the presence of two contiguous glycine residues that adds extra flexibility to the helix in the extracellular region. Deviations from helical structure in TMH3 have also been reported in other GPCRs such as the cholecystokinin CCK1 receptor that also exhibits two kinks, owing to the presence of proline and glycine residues.[67] In contrast, TMH4 presents the smallest conformational change (local RMSD of 0.5 Å shown in Table 2) also exhibiting the small change inside the receptor (global RMSD of 1.6). This stationary behavior upholds it as a good candidate to mediate the oligomerization interface in CB1, as previously postulated.[13,68,69] On the other hand, the TMH6 rotation was accompanied by a 22° straightening (see Fig. 7e). This induce TMH6 to expose its cytoplasmatic end out of the R* core. As a result, a cavity is formed in the cytoplasmatic region of R* as can be deduced from the solvent accessibility change depicted in Table 2.[70] Then again, a deviation from a regular alpha helix and bending is observed in the conserved TMH7 cytoplasmatic region in the R* model (see Fig. 7e). This feature has also been previously established[71,72] and could represent the structural feature that regulates the helix 8 orientation for G-protein activation.[73] In addition, as other authors suggest, the TMH7 bending could be implicated in the ligand binding process.[74]

As a rule drawn from the above comparisons it is possible to separate the conformational changes within TMHs in cytoplasmatic or extracellular, using the toggle switch and polar pocket residues as boundaries (Fig. 8, dash horizontal line and Supplementary Fig. 2). The existence of two functional zones in GPCRs has been proposed before,[75] showing that changes in hydrophobicity and sequence entropy occur close to the core of the lipid bilayer. As can be seen in Figure 7d, all helices

except TMH4 and 6 show increased conservation toward the cytoplasmatic side of the receptor. Through this, a separate conservation–function relationship is envisaged between the extracellular ligand binding region and the cytoplasmatic G-protein interface. The location of the trigger residues $N_{1.50}$, $D_{2.50}$, $F_{3.36}$, $W_{6.48}$, and $N_{7.49}$ in close proximity to the center of the two monolayer lipid inter-phase (see Fig. 8a and b) supports the notion that membrane fluidity could act as a driving force to modify their interactions.[76] In this way, they could operate as mechanosensitive switches in response to lateral pressures on the membrane.[77,78]

3.6. Ligand binding cavities

With the aim to investigate the binding of cannabinergic compounds in the R and R* molecular models, preliminary docking experiments were conducted using three of

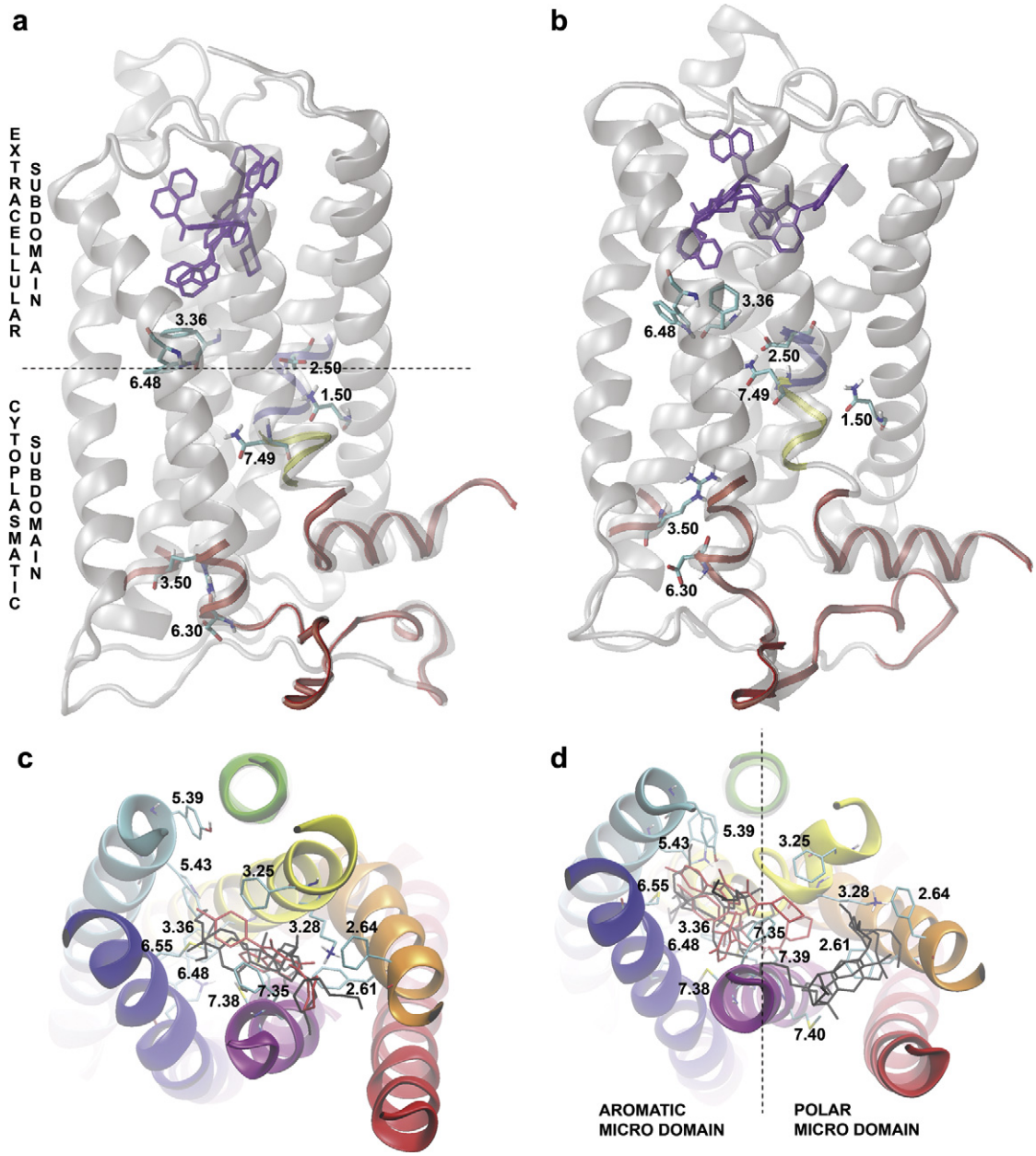

Figure 8. Detailed view of the most important interactions and ligand binding modes identified in the CB1 models (R, a and c), (R*, b and d). On the top, lateral view of developed models. 'Toggle switch', 'ionic lock', and 'polar pocket' residues appear displayed in licorice with labels. Blue and yellow ribbons indicate the TMH2 $LAVAD_{2.50}L$ and TMH7 $NP_{7.50}IIY$ residues, respectively. In red ribbons, the TMH3 $DR_{3.50}Y$ motif, the IC3 C-terminal residues, the cytoplasmatic side of TMH6 and the short helix 8 residues appear. The horizontal dashed line indicates the two monolayer lipid interphase. On the bottom, the extracellular view of developed models. Helices appear colored as follows; TMH1 (red), TMH2 (orange), TMH3 (yellow), TMH4 (green), TMH5 (cyan), TMH6 (dark blue), and TMH7 (magenta). The vertical dashed line delimits the two major ligand binding cavities formed in the activation process. Selected WIN55,212-2, SR-141716A and CP-55940 docking solutions are displayed in magenta, red, and black colors, respectively (see supplementary information). Some relevant residues for ligands binding appear labeled according to Ballesteros and Weinstein nomenclature.[86] Figures were created using VMD v1.8.5.

the most well-known CB1 ligands; the non-classical agonist CP-55940, the aminoalkylindole agonist WIN-55,212-2, and the inverse agonist SR141716a. These molecules were selected as initial approximation based on the broad referred literature in which their binding modes have been proposed (see references[19,44,53,55,79–81]). Selection of binding mode conformations obtained with Autodock was based on the binding energies derived from LUDI and their agreement with previously reported binding modes (see Supplementary Material). The binding sites on the R model were defined by 3 major pockets toward the extracellular core of TMHs bundle, analogous to those reported by Shim & Howlett.[79] Two of them were located proximal to the EC loops surrounded by TMHs 1-2-3-7 and TMHs 3-5-6-7 respectively. The third one was located toward the cytoplasmatic region in a buried cavity among TMHs 3, 6, and 7. The majority of docking solutions occupied two of these pockets at the same time except for the bulky antagonist SR141716a, in which the selected solution occupied the three pockets at once. Conversely, in the R^* model the binding area changes as a consequence of TMHs rearrangements, moving both extracellular pockets apart and defining two major cavities. In this structure, the microdomain constituted by TMHs 3-5-6-7 is the preferred binding site for WIN-55,212-2 and SR141716a ligands.[53] In contrast, two CP-55940 docking solutions were found in the TMHs 1-2-3-7 region close to $K_{3.28}$, a previously reported critical residue in the binding of this smaller non-classical agonist.[82]

On the basis of previous reports, the 'aromatic microdomain' residues $F_{3.25}$, $F_{3.36}$, $W_{4.64}$, $Y_{5.39}$, $W_{5.43}$, and $W_{6.48}$ within TMHs 3-4-5-6 had been proposed as a ligand binding region.[53] In accordance to our results, all but $W_{4.64}$ residues interact with ligands as can be seen in Figure 8 (a detailed description of interactions is provided in the Supplementary Material). In addition, it is possible to define a second binding cavity delimited by the TMHs 1-2-3-7 as the 'polar microdomain'. This definition is based on the close proximity of polar pocket residues to this region and by the presence of the positive residue $K_{3.28}$ identified as an important element in the binding of several ligands.[81,82]

As a general rule derived from these results, the binding pockets defined by CB1 TMHs could be grouped in two major binding cavities or microdomains, as outlined in Figure 8 (vertical dashed line in d). These prototypical subsites locations have also been reported for non-olfactory human GPCRs using chemogenomic analysis[83] and support the allosteric control previously described for the CB1 receptors.[84] This suggests that small-molecule non-classical agonist and possibly classical agonists of CB1 receptor may not necessarily share an overlapping binding site with the most voluminous aromatic AAIs and the diarylpyrazoles antagonist/inverse agonists. However, we cannot rule out the possibility that different classes of ligands have partially overlapping binding pockets as suggested by other authors.[85] In this sense, a fine-tuning of the receptor functional groups would be necessary to determine ligand specificity.

4. Conclusions

The results derived from this theoretical study suggest that the CB1 receptor is composed by structural microdomains that can reorganize its ligand binding sites in response to structural changes. These changes comprise the relaxation of structural constraints and small-scale rearrangements of TMHs that may act in concert to drive the transition among alternate receptor conformations. In this sense, the 7-TMH conformational plasticity constitutes the structural framework that might explain the diversity of ligands with affinity for CB1 receptor. This knowledge could be used in biochemical studies to test the hypotheses of possible ligand binding sites. On the other hand, these experimental findings can then in turn be used to refine our models for virtual screening of chemical databases and rational drug design purposes.

Acknowledgments

We thank Aleksij Aksimentiev for his technical assistance regarding some of the MD simulations methods employed and Julio Caballero for his useful comments. This research was supported in part by the Fundación Chilena para Biología Celular and Fundación Ciencia para la Vida. Angel Gonzalez is economically supported by a CONICYT Ph. D. fellowship.

Supplementary data

Supplementary data associated with this article can be found, in the online version, at doi:10.1016/j.bmc.2008.02.070.

References and notes

1. Palmer, S. L.; Thakur, G. A.; Makriyannis, A. *Chem. Phys. Lipids* **2002**, *121*, 3.
2. Howlett, A. C.; Barth, F.; Bonner, T. I.; Cabral, G.; Casellas, P.; Devane, W. A.; Felder, C. C.; Herkenham, M.; Mackie, K.; Martin, B. R.; Mechoulam, R.; Pertwee, R. G. *Pharmacol. Rev.* **2002**, *54*, 161.
3. Foord, S. M.; Bonner, T. I.; Neubig, R. R.; Rosser, E. M.; Pin, J. P.; Davenport, A. P.; Spedding, M.; Harmar, A. J. *Pharmacol. Rev.* **2005**, *57*, 279.
4. Wise, A.; Gearing, K.; Rees, S. *Drug. Discovery Today* **2002**, *7*, 235.
5. Baldwin, J. M.; Schertler, G. F.; Unger, V. M. *J. Mol. Biol.* **1997**, *272*, 144.
6. Palczewski, K. *Annu. Rev. Biochem.* **2006**, *75*, 743.
7. Cherezov, V.; Rosenbaum, D. M.; Hanson, M. A.; Rasmussen, S. G.; Thian, F. S.; Kobilka, T. S.; Choi, H. J.; Kuhn, P.; Weis, W. I.; Kobilka, B. K.; Stevens, R. C. *Science*, **2007**.
8. Palczewski, K.; Kumasaka, T.; Hori, T.; Behnke, C. A.; Motoshima, H.; Fox, B. A.; Le Trong, I.; Teller, D. C.; Okada, T.; Stenkamp, R. E.; Yamamoto, M.; Miyano, M. *Science* **2000**, *289*, 739.
9. Delos Santos, N. M.; Gardner, L. A.; White, S. W.; Bahouth, S. W. *J. Biol. Chem.* **2006**, *281*, 12896.
10. Choi, G.; Guo, J.; Makriyannis, A. *Biochim. Biophys. Acta* **2005**, *1668*, 1.

11. Rasmussen, S. G.; Choi, H. J.; Rosenbaum, D. M.; Kobilka, T. S.; Thian, F. S.; Edwards, P. C.; Burghammer, M.; Ratnala, V. R.; Sanishvili, R.; Fischetti, R. F.; Schertler, G. F.; Weis, W. I.; Kobilka, B. K. *Nature*, **2007**.
12. Fanelli, F.; De Benedetti, P. G. *Chem. Rev.* **2005**, *105*, 3297.
13. Reggio, P. H. *Aaps J.* **2006**, *8*, E322.
14. Filipek, S.; Teller, D. C.; Palczewski, K.; Stenkamp, R. *Annu. Rev. Biophys. Biomol. Struct.* **2003**, *32*, 375.
15. Kenakin, T. *Trends Pharmacol. Sci.* **2003**, *24*, 346.
16. *Nat. Rev. Drug Discov.*, **2004**, *3*, 575.
17. Deupi, X.; Dolker, N.; Lopez-Rodriguez, M. L.; Campillo, M.; Ballesteros, J. A.; Pardo, L. *Curr. Top. Med. Chem.* **2007**, *7*, 991.
18. Horn, F.; Bettler, E.; Oliveira, L.; Campagne, F.; Cohen, F. E.; Vriend, G. *Nucleic Acids Res.* **2003**, *31*, 294.
19. Salo, O. M.; Lahtela-Kakkonen, M.; Gynther, J.; Jarvinen, T.; Poso, A. *J. Med. Chem.* **2004**, *47*, 3048.
20. Sali, A.; Blundell, T. L. *J. Mol. Biol.* **1993**, *234*, 779.
21. Sippl, M. J. *Proteins* **1993**, *17*, 355.
22. Eisenberg, D.; Luthy, R.; Bowie, J. U. *Methods Enzymol.* **1997**, *277*, 396.
23. Brooks, B.; Bruccoleri, E.; Olafson, B.; States, D.; Swaminathan, S.; Karplus, M. *J. Comput. Chem.* **1983**, *4*, 187.
24. Phillips, J. C.; Braun, R.; Wang, W.; Gumbart, J.; Tajkhorshid, E.; Villa, E.; Chipot, C.; Skeel, R. D.; Kale, L.; Schulten, K. *J. Comput. Chem.* **2005**, *26*, 1781.
25. Aksimentiev, A.; Balabin, I. A.; Fillingame, R. H.; Schulten, K. *Biophys. J.* **2004**, *86*, 1332.
26. Berger, O.; Edholm, O.; Jahnig, F. *Biophys. J.* **1997**, *72*, 2002.
27. Tieleman, D. P.; Forrest, L. R.; Sansom, M. S.; Berendsen, H. J. *Biochemistry* **1998**, *37*, 17554.
28. Li, J.; Edwards, P. C.; Burghammer, M.; Villa, C.; Schertler, G. F. *J. Mol. Biol.* **2004**, *343*, 1409.
29. Lindahl, E.; Hess, B.; Van Der Spoel, D. *J. Mol. Model.* **2001**, *7*, 306.
30. Patra, M.; Karttunen, M.; Hyvonen, M. T.; Falck, E.; Lindqvist, P.; Vattulainen, I. *Biophys. J.* **2003**, *84*, 3636.
31. Berendsen, H. J.; Postma, J. P. M.; van Gunsteren, W. F.; DiNola, A.; Haak, J. R. *J. Chem. Phys.* **1984**, *81*, 3684.
32. Kabsch, W.; Sander, C. *Biopolymers* **1983**, *22*, 2577.
33. Humphrey, W.; Dalke, A.; Schulten, K. *J. Mol. Graph* **1996**, *14*, 33.
34. Schneider, T. D.; Stormo, G. D.; Gold, L.; Ehrenfeucht, A. *J. Mol. Biol.* **1986**, *188*, 415.
35. Ye, K.; Lameijer, E. W.; Beukers, M. W.; Ijzerman, A. P. *Proteins* **2006**, *63*, 1018.
36. Morris, G. M.; Goodsell, D. S.; Halliday, R. S.; Huey, R.; Hart, W. E.; Belew, R. K.; Olson, A. J. *J. Comput. Chem.* **1998**, 1639.
37. Accelrys Inc., San Diego, 2000–2006.
38. Frisch, M. J.; Trucks, G. W.; Schlegel, H. B.; Scuseria, G. E.; Robb, M. A.; Cheeseman, J. R.; Montgomery, J. J. A.; Vreven, T.; Kudin, K. N.; Burant, J. C.; Millam, J. M.; Lyengar, S. S.; Tomasi, J.; Barone, V.; Mennucci, B.; Cossi, M.; Scalmani, G.; Rega, N.; Petersson, G. A.; Nakatsuji, H.; Hada, M.; Ehara, M.; Toyota, K.; Fukuda, R.; Hasegawa, J.; Ishida, M.; Nakajima, T.; Honda, Y.; Kitao, O.; Nakai, H.; Klene, M.; Li, X.; Knox, J. E.; Hratchian, H. P.; Cross, J. B.; Bakken, V.; Adamo, C.; Jaramillo, J.; Gomperts, R.; Stratmann, R. E.; Yazyev, O.; Austin, A. J.; Cammi, R.; Pomelli, C.; Ochterski, J. W.; Ayala, P. Y.; Morokuma, K.; Voth, G. A.; Salvador, P.; Dannenberg, J. J.; Zakrzewski, V. G.; Dapprich, S.; Daniels, A. D.; Strain, M. C.; Farkas, O.; Malick, D. K.; Rabuck, A. D.; Raghavachari, K.; Foresman, J. B.; Ortiz, J. V.; Cui, Q.; Baboul, A. G.; Clifford, S.; Cioslowski, J.; Stefanov, B. B.; Liu, G.; Liashenko, A.; Piskorz, P.; Komaromi, I.; Martin, R. L.; Fox, D. J.; Keith, T.; Al-Laham, M. A.; Peng, C. Y.; Nanayakkara, A.; Challacombe, M.; Gill, P. M. W.; Johnson, B.; Chen, W.; Wong, M. W.; Gonzalez, C.; Pople, J. A. Gaussian, Inc.: Wallingford CT, 2004.
39. Bohm, H. J. *J. Comput. Aided Mol. Des.* **1994**, *8*, 243.
40. Bohm, H. J. *J. Comput. Aided Mol. Des.* **1998**, *12*, 309.
41. Andersson, H.; D'Antona, A. M.; Kendall, D. A.; Von Heijne, G.; Chin, C. N. *Mol. Pharmacol.* **2003**, *64*, 570.
42. Lu, R.; Hubbard, J. R.; Martin, B. R.; Kalimi, M. Y. *Mol. Cell. Biochem.* **1993**, *121*, 119.
43. Fay, J. F.; Dunham, T. D.; Farrens, D. L. *Biochemistry* **2005**, *44*, 8757.
44. Shim, J. Y.; Welsh, W. J.; Howlett, A. C. *Biopolymers* **2003**, *71*, 169.
45. Mukhopadhyay, S.; Shim, J. Y.; Assi, A. A.; Norford, D.; Howlett, A. C. *Chem. Phys. Lipids* **2002**, *121*, 91.
46. Javitch, J. A.; Fu, D.; Liapakis, G.; Chen, J. *J. Biol. Chem.* **1997**, *272*, 18546.
47. Ghanouni, P.; Steenhuis, J. J.; Farrens, D. L.; Kobilka, B. K. *Proc. Natl. Acad. Sci. U.S.A.* **2001**, *98*, 5997.
48. Greasley, P. J.; Fanelli, F.; Rossier, O.; Abuin, L.; Cotecchia, S. *Mol. Pharmacol.* **2002**, *61*, 1025.
49. Ward, S. D.; Hamdan, F. F.; Bloodworth, L. M.; Siddiqui, N. A.; Li, J. H.; Wess, J. *Biochemistry* **2006**, *45*, 676.
50. Ballesteros, J. A.; Jensen, A. D.; Liapakis, G.; Rasmussen, S. G.; Shi, L.; Gether, U.; Javitch, J. A. *J. Biol. Chem.* **2001**, *276*, 29171.
51. Gether, U.; Lin, S.; Ghanouni, P.; Ballesteros, J. A.; Weinstein, H.; Kobilka, B. K. *EMBO J.* **1997**, *16*, 6737.
52. Jensen, A. D.; Guarnieri, F.; Rasmussen, S. G.; Asmar, F.; Ballesteros, J. A.; Gether, U. *J. Biol. Chem.* **2001**, *276*, 9279.
53. McAllister, S. D.; Rizvi, G.; Anavi-Goffer, S.; Hurst, D. P.; Barnett-Norris, J.; Lynch, D. L.; Reggio, P. H.; Abood, M. E. *J. Med. Chem.* **2003**, *46*, 5139.
54. Picone, R. P.; Khanolkar, A. D.; Xu, W.; Ayotte, L. A.; Thakur, G. A.; Hurst, D. P.; Abood, M. E.; Reggio, P. H.; Fournier, D. J.; Makriyannis, A. *Mol. Pharmacol.* **2005**, *68*, 1623.
55. Tuccinardi, T.; Ferrarini, P. L.; Manera, C.; Ortore, G.; Saccomanni, G.; Martinelli, A. *J. Med. Chem.* **2006**, *49*, 984.
56. Filizola, M.; Wang, S. X.; Weinstein, H. *J. Comput. Aided Mol. Des.* **2006**, *20*, 405.
57. Fanelli, F.; De Benedetti, P. G. *J. Comput. Aided Mol. Des.* **2006**, *20*, 449.
58. Nebane, N. M.; Kellie, B.; Song, Z. H. *FEBS Lett.* **2006**, *580*, 5392.
59. Singh, R.; Hurst, D. P.; Barnett-Norris, J.; Lynch, D. L.; Reggio, P. H.; Guarnieri, F. *J. Pept. Res.* **2002**, *60*, 357.
60. McAllister, S. D.; Hurst, D. P.; Barnett-Norris, J.; Lynch, D.; Reggio, P. H.; Abood, M. E. *J. Biol. Chem.* **2004**, *279*, 48024.
61. Zhou, W.; Flanagan, C.; Ballesteros, J. A.; Konvicka, K.; Davidson, J. S.; Weinstein, H.; Millar, R. P.; Sealfon, S. C. *Mol. Pharmacol.* **1994**, *45*, 165.
62. Sealfon, S. C.; Chi, L.; Ebersole, B. J.; Rodic, V.; Zhang, D.; Ballesteros, J. A.; Weinstein, H. *J. Biol. Chem.* **1995**, *270*, 16683.
63. Scheer, A.; Fanelli, F.; Costa, T.; De Benedetti, P. G.; Cotecchia, S. *EMBO J.* **1996**, *15*, 3566.
64. Gether, U. *Endocr. Rev.* **2000**, *21*, 90.
65. Nie, J.; Lewis, D. L. *J. Neurosci.* **2001**, *21*, 8758.
66. Fritze, O.; Filipek, S.; Kuksa, V.; Palczewski, K.; Hofmann, K. P.; Ernst, O. P. *Proc. Natl. Acad. Sci. U.S.A.* **2003**, *100*, 2290.

67. Archer, E.; Maigret, B.; Escrieut, C.; Pradayrol, L.; Fourmy, D. *Trends Pharmacol. Sci.* **2003**, *24*, 36.
68. Wager-Miller, J.; Westenbroek, R.; Mackie, K. *Chem. Phys. Lipids* **2002**, *121*, 83.
69. Mackie, K. *Life Sci.* **2005**, *77*, 1667.
70. Angelova, K.; Fanelli, F.; Puett, D. *J. Biol. Chem.* **2002**, *277*, 32202.
71. Konvicka, K.; Guarnieri, F.; Ballesteros, J. A.; Weinstein, H. *Biophys. J.* **1998**, *75*, 601.
72. Berlose, J. P.; Convert, O.; Brunissen, A.; Chassaing, G.; Lavielle, S. *Eur. J. Biochem.* **1994**, *225*.
73. Mukhopadhyay, S.; Cowsik, S. M.; Lynn, A. M.; Welsh, W. J.; Howlett, A. C. *Biochemistry* **1999**, *38*, 3447.
74. Kapur, A.; Hurst, D. P.; Fleischer, D.; Whitnell, R.; Thakur, G. A.; Makriyannis, A.; Reggio, P. H.; Abood, M. E. *Mol. Pharmacol.* **2007**, *71*, 1512.
75. Imai, T.; Fujita, N. *Proteins* **2004**, *56*, 650.
76. Lee, A. G. *Biochim. Biophys. Acta* **2004**, *1666*, 62.
77. Gudi, S.; Nolan, J. P.; Frangos, J. A. *Proc. Natl. Acad. Sci. U.S.A.* **1998**, *95*, 2515.
78. Chachisvilis, M.; Zhang, Y. L.; Frangos, J. A. *Proc. Natl. Acad. Sci. U.S.A.* **2006**, *103*, 15463.
79. Shim, J. Y.; Howlett, A. C. *J. Chem. Inf. Model.* **2006**, *46*, 1286.
80. Hurst, D.; Umejiego, U.; Lynch, D.; Seltzman, H.; Hyatt, S.; Roche, M.; McAllister, S.; Fleischer, D.; Kapur, A.; Abood, M.; Shi, S.; Jones, J.; Lewis, D.; Reggio, P. *J. Med. Chem.* **2006**, *49*, 5969.
81. Hurst, D. P.; Lynch, D. L.; Barnett-Norris, J.; Hyatt, S. M.; Seltzman, H. H.; Zhong, M.; Song, Z. H.; Nie, J.; Lewis, D.; Reggio, P. H. *Mol. Pharmacol.* **2002**, *62*, 1274.
82. Song, Z. H.; Bonner, T. I. *Mol. Pharmacol.* **1996**, *49*, 891.
83. Surgand, J. S.; Rodrigo, J.; Kellenberger, E.; Rognan, D. *Proteins* **2006**, *62*, 509.
84. Price, M. R.; Baillie, G. L.; Thomas, A.; Stevenson, L. A.; Easson, M.; Goodwin, R.; McLean, A.; McIntosh, L.; Goodwin, G.; Walker, G.; Westwood, P.; Marrs, J.; Thomson, F.; Cowley, P.; Christopoulos, A.; Pertwee, R. G.; Ross, R. A. *Mol. Pharmacol.* **2005**, *68*, 1484.
85. Shim, J. Y.; Collantes, E. R.; Welsh, W. J.; Subramaniam, B.; Howlett, A. C.; Eissenstat, M. A.; Ward, S. J. *J. Med. Chem.* **1998**, *41*, 4521.
86. Ballesteros, J. A.; Weinstein, H. *Methods Neurosci.* **1995**, *25*, 366.